Rubber Toughening of Polyamide 6/Organoclay Nanocomposites Obtained by Melt Blending

F. Baldi,[1] F. Bignotti,[1] G. Tieghi,[2] T. Riccò[1]

[1]*Dipartimento di Chimica e Fisica per l'Ingegneria e per i Materiali, Università di Brescia, Via Valotti 9, I-25123 Brescia, Italy*
[2]*Dipartimento di Chimica, Materiali e Ingegneria Chimica "Giulio Natta," Politecnico di Milano, Piazza Leonardo da Vinci 32, I-20133 Milano, Italy*

Received 29 December 2004; accepted 8 April 2005
DOI 10.1002/app.22955
Published online 19 January 2006 in Wiley InterScience (www.interscience.wiley.com).

ABSTRACT: Rubber toughening of polyamide 6 (PA6)/layered-silicate nanocomposites was investigated. Different systems were prepared via melt blending according to different formulations. Wide-angle X-ray diffraction and transmission electron microscopy analyses showed that the nanocomposites had an appreciable degree of exfoliation. A linear elastic fracture mechanics approach was applied to characterize the material fracture behavior in dry conditions, whereas, because of the considerable ductility exhibited by the samples in the wet state, an elastic–plastic approach based on the essential work of fracture methodology was employed. In the absence of rubber, the presence of silicate layers makes the material fracture resistance decrease relative to neat polymer, depending on the degree of humidity. The results showed that the toughening action of rubber strongly depends on the degree of humidity of the material, at least for the rubber contents considered in this study (lower than 10 wt %). In particular, in slightly wet conditions, it was found that the addition of small amounts of rubber increased the fracture resistance of PA6/layered-silicate nanocomposites without appreciably impairing the material stiffness. Thus, the results indicated that, for the given humidity conditions, a good balance between stiffness and toughness was obtainable by employing a suitable ratio of rubber to layered-silicate content. J Appl Polym Sci 99: 3406–3416, 2006

Key words: nanocomposites; polyamides; organoclay; toughness; fracture

INTRODUCTION

Since the early 1990s, when the peculiar properties of a new class of polymer composites, polyamide 6 (PA6)/phyllosilicate nanocomposites, were first reported,[1] organoclays (organo-modified phyllosilicates) have been employed as the dispersed phase in the preparation of polymer/layered-silicate nanocomposites (PLSN), where the organoclay platelets are nanometrically dispersed in the polymer matrix. Much interest has been focused on understanding and developing PLSN with thermoplastic, thermosetting, or elastomeric matrices, because the addition of small amounts (typically from 1 to 10 wt %) of organo-modified phyllosilicates produces a significant improvement in a broad spectrum of properties in comparison with neat polymer.[2] It has been pointed out that the incorporation of silicate layers into a polymeric matrix improves the mechanical properties, thermal stability, and reaction to fire of the material, depending on both the dispersion efficiency and the type of clay compatibilizer. Moreover, in contrast with traditional microcomposites, the addition of small quantities of organoclay permits the processability and recyclability of the material to be little modified with respect to the polymer matrix.

Because of the very promising results evidenced by the first systems studied, PA6/layered-silicate nanocomposites prepared by various techniques, such as in situ polymerization and melt blending, have been investigated.[3–6] The results have shown that silicate layers increase both stiffness and strength of PA6 more efficiently than do microscale particles. Furthermore, it has been claimed that the presence of silicate layers does not appreciably influence the Charpy and Izod impact strength of PA6 nanocomposites prepared both via in situ polymerization and melt blending.[2,7] Despite this, it has been noticed that the incorporation of silicate layers decreases ductility, depending on the type of organoclay compatibilizer, as shown by the drop of elongation at break observed with increasing organoclay content.[8–10] Moreover, recent studies on the fracture behavior of polyamide 66 (PA66)–based nanocomposites, by the application of fracture mechanics testing methods, have shown that in PA66 the presence of silicate layers produces a pronounced embrittlement that is intrinsic to the material.[11,12] Preliminary data obtained by the authors of the present

Correspondence to: F. Baldi (baldi@ing.unibs.it).

article about the fracture behavior of PA6/layered-silicate nanocomposites prepared by melt blending confirmed this filler-induced embrittlement effect.

The aim of the present work was to investigate the possibility of improving the fracture resistance of PA6/layered-silicate systems by rubber toughening. The fracture behavior of rubber-modified PA6/layered-silicate nanocomposites prepared via melt compounding according to different formulations was studied. To minimally reduce the reinforcement promoted by the silicate layers, nanocomposites modified by having a low rubber content were prepared. Their morphology was investigated and their tensile properties measured in both dry and wet conditions. The fracture behavior of the rubber-modified nanocomposites was analyzed in different humidity conditions by fracture mechanics testing methods and compared with that of both neat polymer and nanocomposites devoid of rubbery particles. For characterization of the materials in dry conditions, a linear elastic fracture mechanics (LEFM) approach[13] was used, whereas, because of the ductility of the wet samples examined, an elastic–plastic approach based on the methodology of the essential work of fracture[14] was applied.

The essential work of fracture (EWF) method, successfully applied to ductile polymers, was first developed by Broberg,[15] who proposed that the total fracture energy (W_f) spent to bring a precracked body to complete failure could be partitioned in two contributions:

$$W_f = W_e + W_p \tag{1}$$

where W_e is the essential work of fracture dissipated in an inner fracture process zone (IFPZ) and W_p is the nonessential work of fracture dissipated in an outer plastic deformation zone (OPDZ; see Fig. 1). In plane stress conditions the essential work of fracture, which represents the energy dissipated inside the fracture process zone, should be proportional to the ligament length of the test piece (l), whereas the nonessential work of fracture, associated with the energy required to create the outer plastic zone, should be proportional to l^2 as follows:

$$W_f = w_f lB = w_e lB + \beta w_p l^2 B \tag{2}$$

and

$$w_f = w_e + \beta w_p l \tag{3}$$

where B is the specimen thickness, β is a shape factor depending on both the material and the geometry of the body, and w_f, w_e, and w_p are the specific total, essential, and nonessential work of fracture, respectively. For a given specimen thickness, w_e represents an intrinsic material property.[16] According to eq. (3),

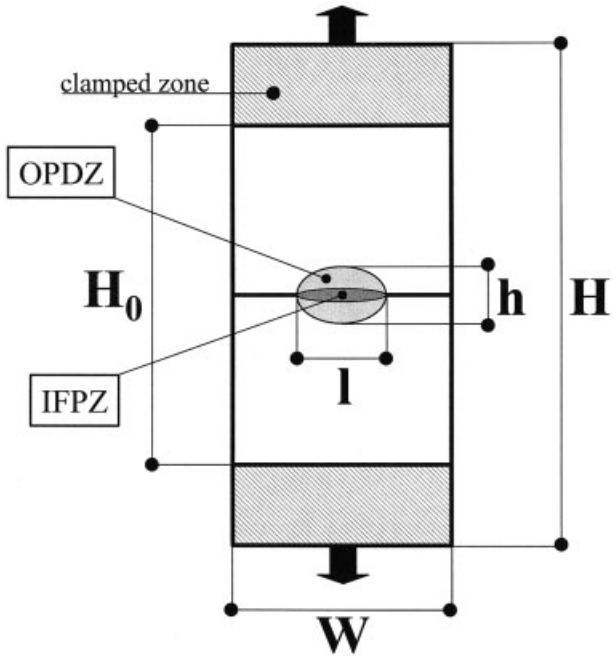

Figure 1 Double-edge notched in tension (DENT) specimen used for the essential work of fracture tests; a schematic representation of the different zones is shown.

w_e and βw_p are determined by a linear interpolation of a series of experimental data of w_f obtained by testing specimens having different ligament lengths. Recent studies[17–19] have shown that the total fracture energy, W_f, may be divided into two components: the work of fracture spent for yielding the ligament region, W_y, and the work of fracture for necking and subsequent tearing of the ligament region, W_{nt}. Considering the yielding and necking/tearing contributions to w_f:

$$w_y = W_y / lB = w_{ey} + \beta_y w_{py} l \tag{4}$$

$$w_{nt} = W_{nt} / lB = w_{ent} + \beta_{nt} w_{pnt} l \tag{5}$$

where w_{ey} and w_{ent} are the yielding and necking/tearing components of the specific essential work of fracture, w_e, respectively; w_{py} and w_{pnt} are the yielding and necking/tearing related parts of the specific nonessential work of fracture, w_p, respectively, and β_y and β_{nt} are the yielding and necking/tearing related parts of the shape factor, β, respectively.

EXPERIMENTAL

Materials

The materials examined were prepared by Radici Novacips SpA (Villa d'Ogna, Bergamo, Italy) and supplied in the form of dumbbell specimens (according to ISO 527), 80 × 10 × 4 mm bars (according to ISO 179), and 60 × 60 × 1 mm plaques (according to ISO 6603),

TABLE I
Tensile Properties of the Various Materials in Both Dry and Highly Wet Conditions

PA6/MM/R[a]		Dry[b]			Highly wet[c]	
% MM	% R	Young's modulus (MPa)	Yield stress (MPa)	Elongation at break (%)	Young's modulus (MPa)	Yield stress (MPa)
0	0	2870 ± 50	65 ± 2.1	70 ± 13	530 ± 15	29 ± 0.2
0	5	2490 ± 40	61 ± 0.6	44 ± 6	450 ± 15	25.3 ± 0.1
0	10	2190 ± 40	51.4 ± 0.1	61 ± 3	410 ± 14	22.2 ± 0.1
4	0	4100 ± 150	84 ± 0.5	4.8 ± 0.2	1000 ± 70	32.1 ± 0.1
4	5	3400 ± 70	66 ± 0.7	6 ± 1	870 ± 30	27.6 ± 0.2
4	10	2900 ± 60	56.3 ± 0.3	7.5 ± 0.3	730 ± 35	24 ± 0.2
6	0	4700 ± 190	—[d]	3.6 ± 0.1	1100 ± 60	31.97 ± 0.01
6	5	3800 ± 50	—[d]	3.3 ± 0.1	1045 ± 4	27.4 ± 0.3
6	10	3370 ± 40	55 ± 0.4	3.5 ± 0.2	930 ± 25	23.5 ± 0.2

[a] R, rubber.
[b] 0.1–0.2 wt % water content.
[c] 8–9 wt % water content.
[d] No yielding was observed.

prepared via injection molding. The PA6 employed had a weight-average molecular weight of 39,000 g/mol. The organoclay was Nanomer I.30TC from Nanocor (Arlington Heights, IL), which is an organomodified montmorillonite (MM) containing about 70 wt % clay. The nanocomposites were produced via melt blending: a master batch (20 wt % organoclay), previously prepared via melt compounding, was diluted in PA6 matrix by a corotating twin-screw extruder. The rubber-modified systems were obtained compounding the master batch, PA6, and an ethylene-*co*-propylene maleated rubber.

The materials investigated can be classified as follows: base system (PA6), binary systems (PA6 with either organoclay or rubber added), and ternary systems (PA6 with both organoclay and rubber added). As shown in Table I, three organoclay contents (0, 4, and 6 wt %) and three rubber contents (0, 5, and 10 wt %) were employed. Small rubber contents were chosen to avoid significantly impairing the stiffness of the nanocomposites.

Because the mechanical properties of PA6 are strongly influenced by water content,[20] in this study the behavior of the various systems was explored at three humidity levels: dry (about 0.1–0.2 wt % water content relative to the neat PA6), slightly wet (about 1–2 wt % water content relative to the neat PA6), and highly wet (about 8–9 wt % water content relative to the neat PA6). These humidity contents were obtained as reported elsewhere.[21]

Morphological analyses

Wide-angle X-ray diffraction (WAXD) patterns were recorded by a Philips PW1710 diffractometer, using Cukα radiation, in the 2°–50° 2θ range. The specimens were obtained from the 60 × 60 × 1 mm plaques.

The morphology of the materials was detected by both transmission and scanning electron microscopy (TEM and SEM, respectively).

For TEM analyses a Philips CM120, operating at an accelerating voltage of 80 kV, was used. The samples were ultramicrotomed at cryogenic conditions with a thickness of about 100 nm. Staining was not used. Clay platelets appear dark in TEM images.

For SEM analyses a LEO 1525 high-resolution scanning electron microscope, operated at a beam energy of 0.7 keV in order to prevent electrostatic charging of the unprepared specimen, was employed. The secondary-electron images were provided by an Everhart–Thornley detector. The analyses were performed on cryogenic fracture surfaces obtained by breaking the samples at liquid nitrogen atmosphere, and the rubbery phase was selectively etched out by xylene for 30 min at 80°C.

Uniaxial tensile tests

Tensile tests were performed on dumbbell specimens using an Instron dynamometer (model 3366) equipped with a 10 kN load cell. The initial length of the narrow section of the test specimen was about 80 mm and its cross section 10 × 4 mm. All the tests were performed at room temperature using a crosshead speed of 2 mm/min. Measurement of the Young's modulus was performed with a strain-gauge extensometer whose gauge length was 25 mm. All the properties were evaluated on an average of at least three specimens.

Fracture tests

Fracture measurement was performed with an Instron dynamometer (model 3366) equipped with a 500 N

load cell for K_{Ic} testing and a 10 kN load cell for the essential work of fracture testing.

The sharp notches were produced on the specimens for both K_{Ic} testing and the essential work of fracture testing by means of a notching machine by Ceast SpA (Torino, Italy).

K_{Ic} was determined according to the procedure proposed by ESIS TC4 (Technical Committee 4 "Plastics, Adhesives and Composites")—now ISO 13586[13]—by flexural tests carried out on single-edge notched in bending [SE(B)] specimens (40-mm span), prepared from bars with dimensions of 80 × 10 × 4 mm, at a crosshead speed of 10 mm/min and at room temperature.

Plane stress EWF was evaluated for each material using the multispecimen technique proposed by ESIS TC4.[14] For each material a series of 25 double-edge notched tension specimens (DENT)—see Figure 1 for geometrical details—having different ligament lengths was tested. Each specimen was prepared by cutting a rectangular coupon of 60 × 29 mm from a plaque. Each coupon was cut from the center of the plaque in such a way that the long side of the specimen was aligned with injection direction. The coupons were then notched to produce DENT specimens with a nominal ligament length ranging from 4 to 14 mm. The ligament length ranged between 3B (B is the thickness of the specimen) and W/2 to ensure plane stress conditions avoiding edge effects. Each specimen was then tested to complete failure with a dynamometer that had a distance of H_0 = 40 mm between the grips using a crosshead speed of 2 mm/min at room temperature. For each specimen the load-versus-displacement curve was recorded, and the absorbed work of fracture (W_f) was calculated by integration of the area under the curve. The real ligament length (l) and the height of the plastic zone (h) of each specimen were measured on the fractured specimen using an optical traveling microscope. For each series of specimens the stress criterion proposed by the ESIS protocol was applied "to ensure greater likelihood of fracture occurring under plane stress conditions and to remove data where fracture has occurred prior to full ligament yielding."[14] According to this criterion, data with maximum stress, σ_{max} (defined as the ratio between the maximum load measured during the test and the ligament section), greater than 1.1 $\sigma_{max,m}$ and less than 0.9 $\sigma_{max,m}$ (where $\sigma_{max,m}$ is the mean maximum stress averaged on all the data acquired for the series under investigation) were rejected. Then, on the specific total work of fracture versus ligament diagram, data having values more than two times the standard deviation from the best-fit line were eliminated from the analysis. Having rejected these points, a final least-squares linear regression was applied to the remaining data in order to determine the intercept, w_e (with the 95% confidence limits on the intercept), and the slope, βw_p.

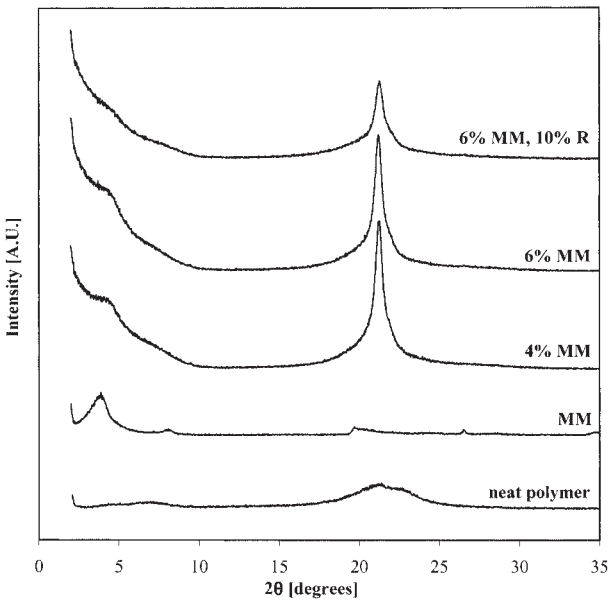

Figure 2 WAXD patterns of PA6, organoclay, and selected nanocomposites (R, rubber).

The remaining data also were used for the evaluation of the components of the specific essential work of fracture for yielding, w_{ey}, and for necking/tearing, w_{ent}.

RESULTS AND DISCUSSION

Morphology

The X-ray diffraction patterns of PA6, organoclay, binary systems of 4% and 6% MM, and the ternary system of 6% MM and 10% rubber are shown in Figure 2. The WAXD pattern of the organo-modified montmorillonite shows a characteristic peak at 3.9° corresponding to a basal spacing of 22.9 Å. It is known that the addition of MM to a polymer matrix through melt blending produces exfoliation and intercalation of the organoclay, which results in broadening and spacing increase of its characteristic peak, respectively. In the WAXD pattern of the PA6/layered-silicate nanocomposites reported in Figure 2, this peak could only be detected as a shoulder of the intensity profile in the region of the lowest 2θ angles. This shoulder appeared to be less pronounced in the pattern of the 6% MM nanocomposite than in that of the 4% MM nanocomposite, indicating a higher degree of exfoliation in the former. Moreover, the shoulder was hardly detectable in the WAXD pattern of the system with a 6% MM and 10% rubber content, suggesting that the presence of rubber increased the degree of exfoliation of the organoclay. Further, it could be observed that although pure PA6 typically shows two peaks, at 21.4° and 22.8°, corresponding to the γ and α crystalline phases, respectively, the binary and ternary

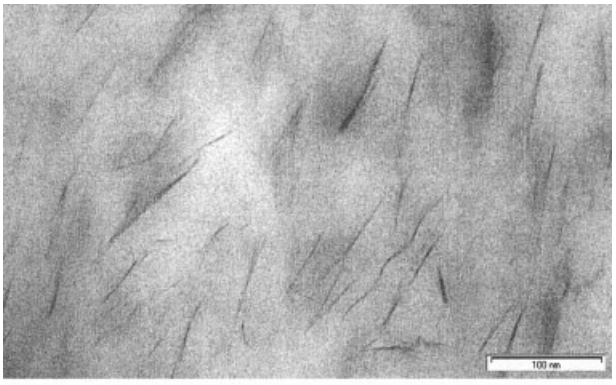

(a)

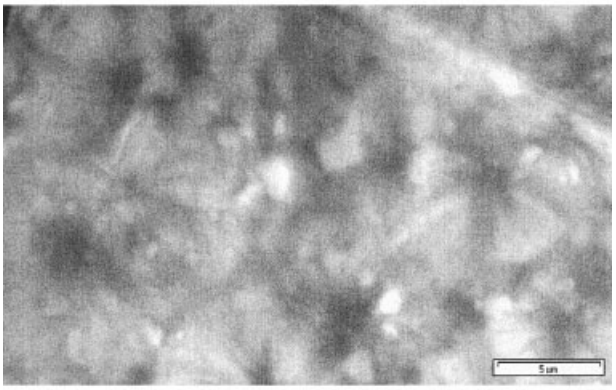

(b)

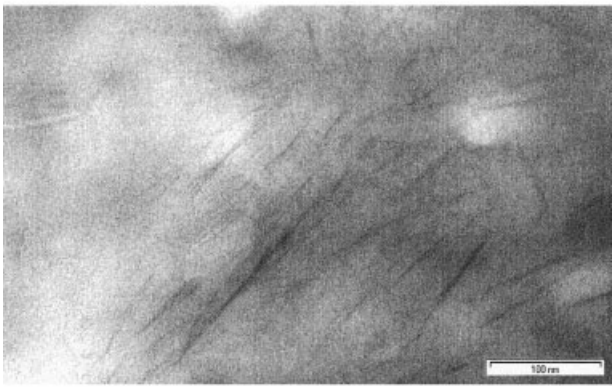

(c)

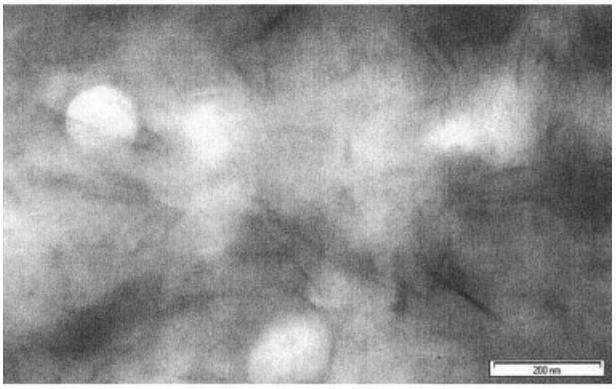

(d)

systems showed only the γ phase peak at 21.4°. This topic will be discussed in another article,[21] which will take up the structure of PA6/layered-silicate nanocomposites.

The TEM image of the nanocomposite containing 6% MM [Fig. 3(a)] shows an appreciable level of clay exfoliation. In the binary system containing 10% rubber [Fig. 3(b)], the presence of polyamide spherulites surrounding white rubber particles can be clearly seen. In the ternary system containing 6% MM and 10% rubber [Fig. 3(c,d)], the montmorillonite exfoliation level is comparable to that of the nanocomposite containing 6% MM, whereas no evidence for a spherulitic morphology was found. In agreement with the results reported by Khatua et al.[22] for PA6-based nanocomposites modified with ethylene-*ran*-propylene rubber, clay platelets were not detected in the rubber domains. Therefore, even if it cannot be excluded that a minor amount of clay was incorporated in the rubbery dispersed phase, it may be assumed that almost all platelets were contained in the polyamide matrix. This can be accounted for by the higher polarity of PA6 in comparison with the rubber, which suggests a higher miscibility of the former with organoclay.

By comparing the SEM image of the binary system at 10% rubber [Fig. 4(a)] with that of the ternary system containing 6% MM and 10% rubber [Fig. 4(b)], it could be observed that the presence of the organoclay did not seem to modify substantially the dispersion of the rubber particles. However, a more accurate analysis of the effects of the presence of the organoclay on the dispersed rubber domain size in the ternary systems is necessary, a work that is in progress.

Stress–strain behavior

Typical stress–strain curves of PA6/layered-silicate nanocomposites, rubber-modified PA6, and rubber modified PA6/layered-silicate nanocomposites in dry conditions are shown in Figure 5. Table I summarizes the results of the tensile properties for the various materials in both dry and highly wet conditions.

The stress–strain curves of PA6/layered-silicate nanocomposites presented in Figure 5(a) show that in dry conditions the addition of silicate layers strongly modified the mechanical behavior of PA6. It increased the yield stress and drastically reduced the elongation at break. Further, with a 6% MM content, no yielding was observed, and the material reached breakage at

Figure 3 TEM images of (a) nanocomposite containing 6% MM; (b) rubber-modified PA6 containing 10% rubber; (c), (d) rubber-modified nanocomposite containing 6% MM and 10% rubber, respectively. The white areas in (b)–(d) correspond to rubber particles.

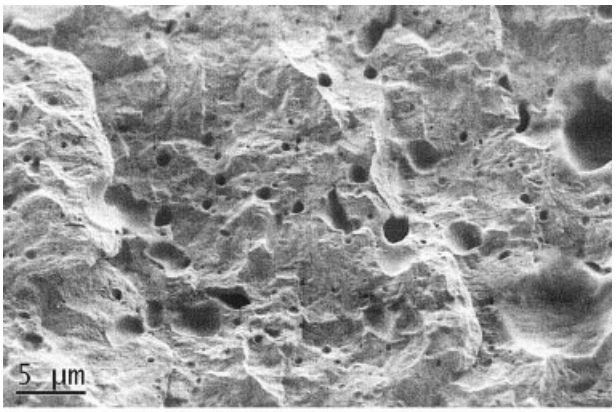

(a)

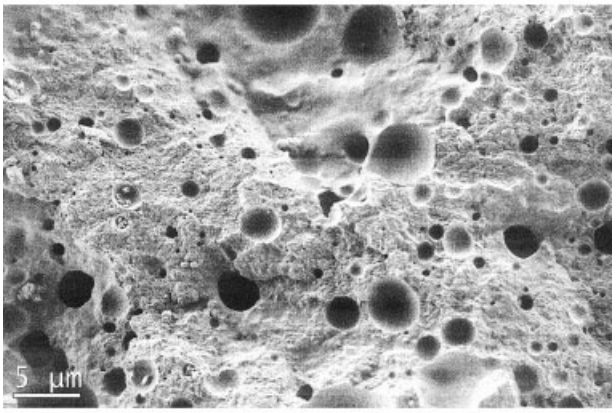

(b)

Figure 4 SEM images of (a) rubber-modified PA6 containing 10% rubber; (b) rubber-modified nanocomposite at 6% MM and 10% rubber.

very low strain values. This behavior could indicate that specific PA6/silicate layer interactions drastically modified the deformation mechanisms of the material, hindering the achievement of large strains.

In dry conditions the addition of rubber particles to PA6 [see Fig. 5(a)] produced a decrease in the yield stress without substantially modifying the elongation at break.

The addition of the rubbery phase to the nanostructured systems still produced a reduction in the yield stress of the material [see Fig. 5(b)] that was more pronounced than that observed for neat PA6: the addition of 10% rubber to the nanocomposite containing 4% MM reduced yield stress by 33%, whereas for neat PA6 a decrease of 21% was observed. The incorporation of rubber into the nanocomposites produced some improvement of the elongation at break for the samples containing 4% MM, whereas it left this property substantially unaffected for the samples containing 6% MM.

In highly wet conditions the increase in yield stress induced by the presence of the nanofillers for both PA6 and rubber modified systems was considerably reduced in comparison with that shown in dry conditions (see Table I).

Further, the results showed that the incorporation of silicate layers in the PA6 matrix produced a remarkable increase in the material stiffness. The addition of 6% MM to PA6 caused a Young's modulus increase of 64% in dry conditions and a 108% increase in highly wet conditions. In contrast, the addition of rubber particles caused a reduction in the Young's modulus. In the rubber-modified PA6/layered-silicate nanocomposites the reinforcement induced by the nanoscopic particles was partially contrasted by the presence of the elastomeric phase, which produced a slight decrease in the Young's modulus. Despite this, the enhanced Young's modulus produced by the silicate layers in the PA6 matrix always remained rather pronounced compared with that in the neat PA6 (see Fig. 6).

Fracture behavior

The loading curves recorded in the LEFM fracture tests on dry samples are presented in Figure 7, and the values of the critical stress intensity factor, K_{Ic}, and the

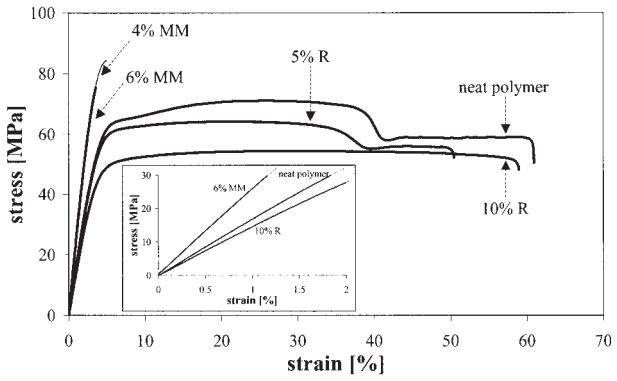

(a)

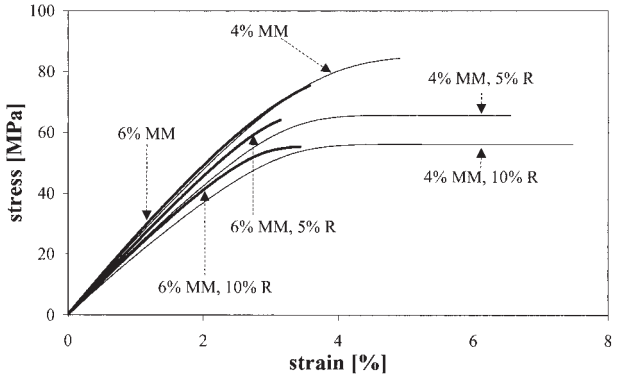

(b)

Figure 5 Typical stress–strain curves (in dry conditions) of (a) rubber-modified PA6 systems and PA6/layered-silicate nanocomposites, (b) rubber-modified PA6-based nanocomposites (R, rubber).

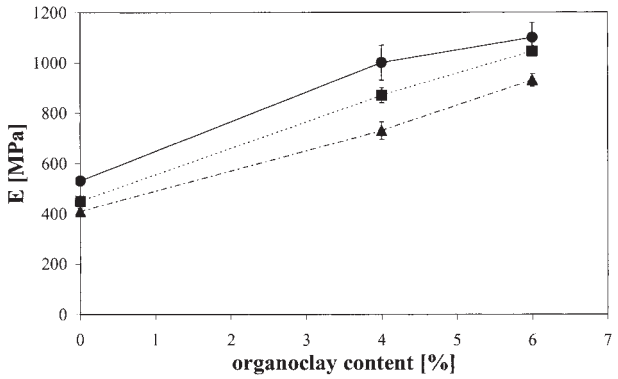

Figure 6 Young's modulus (in highly wet conditions) as a function of organoclay content (●, 0% rubber; ■, 5% rubber; ▲, 10% rubber).

uncorrected fracture energy, G_Q, at fracture initiation, are reported in Table II. The loading curves exhibited quite different shapes, with both silicate and rubber content varying. In particular, the addition of the nanofiller to the PA6 matrix caused a pronounced reduction in the fracture toughness of the material, and the rubber-modified PA6 systems showed very ductile behavior accompanied by a remarkable degree of nonlinearity prior to the attainment of the maximum load, thus violating the LEFM applicability conditions [see Fig. 7(a)]. The addition of the rubbery phase to the nano-structured systems did not result in an appreciable increase in the fracture toughness measured at fracture initiation [see Fig. 7(b)], although for the systems containing 4% MM, it inhibited the catastrophic propagation of the fracture observed for PA6 and the other nanostructured systems examined.

Flexural tests carried out on SE(B) specimens in both slightly and highly wet conditions, using the same testing configuration, highlighted that at a slow rate the LEFM approach could not be used for the correct characterization of the wet materials (results not shown). In both slightly and highly wet conditions all the systems showed very ductile behavior. In particular, in highly wet conditions, the differences in the fracture behavior of the various materials could not be clearly recognized, indicating that the toughening effect of water predominated. To correctly study the fracture behavior of the materials in slightly wet conditions, an elastic–plastic fracture mechanics methodology, the essential work of fracture method, was applied.

The EWF tests on DENT specimens of the several types of materials analyzed in the present study produced load-versus-displacement curves of the type shown in Figure 8. The curves, which refer to specimens of the same material (PA6) with different ligament lengths [Fig. 8(a)] and to nominally identical specimens of different materials [Fig. 8(b)], showed that failure of the samples occurred by ductile tearing preceded by yielding and necking of the yielded region. Visual observations of the specimens during the tests indicated that full ligament yielding occurred prior to crack growth and that the full yielding of the ligament region occurred at maximum load. The necking of the fully yielded region led to the load drop after maximum, though it was scarcely pronounced for several materials. The diagrams shown in Figure 8(a) highlight the expected homothetic behavior of PA6 with varying ligament lengths up to the displacement at break. Geometrical similarity of the curves as a function of the ligament length, which is a basic requirement for determining w_e, also was observed for the other materials investigated. Figure 8(b) shows that the addition of rubber particles to PA6 did not modify appreciably the load-versus-displacement trace of the polymer, whereas the incorporation of the nanoscopic particles into the PA6 matrix reduced (proportional to silicate layer content) the displacement at break and increased both the maximum load and the stiffness of the specimen. The curves referring to rubber-modified PA6/layered-silicate nanocomposites did not show significant differences from those of the corresponding nanocomposites devoid of a rubbery phase.

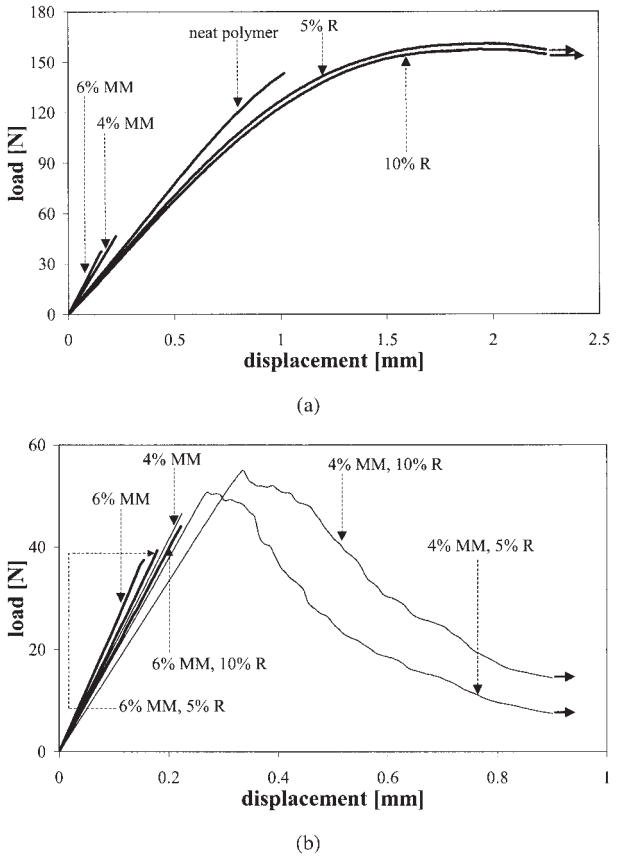

Figure 7 Loading curves recorded in fracture tests (in dry conditions) on: (a) rubber-modified PA6 systems and PA6/layered-silicate nanocomposites, (b) rubber-modified PA6-based nanocomposites (R, rubber).

TABLE II
LEFM Results for the Various Materials in Dry Conditions

PA6/MM/R[a]		LEFM validity	K_Q	Size criteria for	
% MM	% R	condition	(MPa · m$^{0.5}$)	$K_{Ic} = K_Q$	G_Q (kJ/m^2)
0	0	satisfied	4 ± 0.2	not satisfied	7.7 ± 0.48
0	5	not satisfied	—	—	—
0	10	not satisfied	—	—	—
4	0	satisfied	1.4 ± 0.06	satisfied	0.54 ± 0.02
4	5	satisfied	1.6 ± 0.09	satisfied	0.9 ± 0.18
4	10	satisfied	1.6 ± 0.4	satisfied	1.1 ± 0.18
6	0	satisfied	1.0 ± 0.07	not checked[b]	0.3 ± 0.04
6	5	satisfied	1.1 ± 0.01	not checked[b]	0.36 ± 0.01
6	10	satisfied	1.2 ± 0.02	satisfied	0.51 ± 0.01

[a] R, rubber.
[b] No yield stress data available.

By plotting w_f versus l of each series of specimens, w_e and βw_p were determined according to the EWF protocol.[14] For the evaluation of w_{ey} and w_{ent}, the total work of fracture, W_f (area under the load-vs.-displacement curve up to the displacement at break) was divided into two parts for each specimen: (1) work of fracture for yielding, W_y (area under the load-vs.-displacement curve up to the displacement corresponding to the maximum load—where the full yielding of the ligament region occurred); and (2) work of fracture for necking/tearing, W_{nt} (remaining area under the load *vs* displacement curve). From the w_y-versus-l and w_{nt}-versus-l plots, respectively, the two corresponding essential values were determined by extrapolation [see eqs. (4) and (5)].

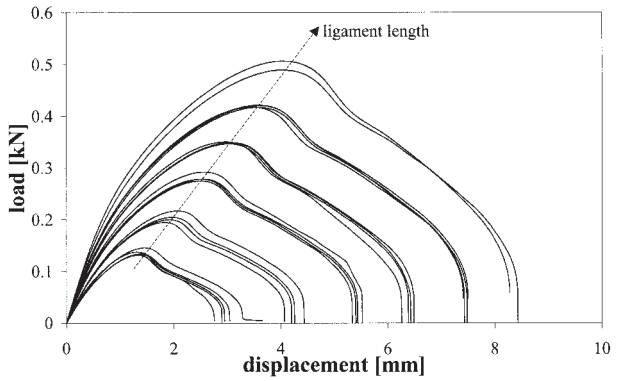

(a)

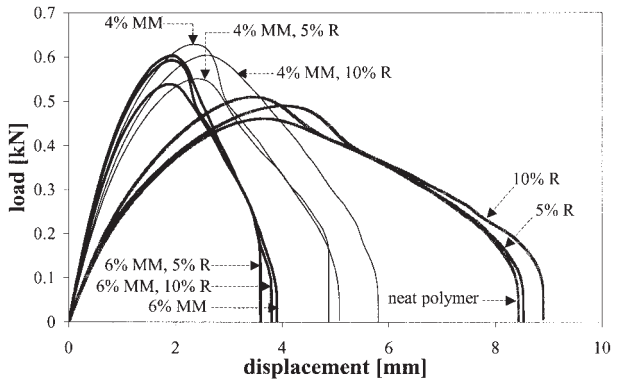

(b)

Figure 8 Typical load versus displacement curves for DENT specimens in essential work of fracture tests (in slightly wet conditions): (a) effect of ligament length for PA6, (b) effect of organoclay and rubber content (specimens having the same ligament length l = 14 mm); R, rubber.

The value of β (shape factor) was determined by using the relation between h (plastic zone height) and l as recommended in the ESIS protocol of 1993[23] and described previously.[24–26] Further, visual inspection of the broken specimens identified the plastic region as being eye shaped[27,28] for all the materials analyzed in the present study. For this shape, which results from the intersection of two parabolas, the following expression could be derived:

$$h = 1.5 \cdot \beta \cdot l \tag{6}$$

where h is the height of the plastic zone (taking into account the two parts of the broken specimen) and l is the ligament. By plotting h versus l and calculating the least-squares regression line, β was obtained from the slope of the line. Once the shape factor was determined for each material, w_p could be easily deduced. It is worth mentioning that, given that β was deduced indirectly from the values of h (not easily measured in all the materials), experimental error may have been important.

The results of EWF testing of the different materials are summarized in Figures 9 and 10 and listed in Table III.

The results show that even if the presence of water molecules adsorbed by PA6 improved the fracture behavior of the nanocomposites in comparison with what was observed in dry conditions, the addition of the nanofiller to the PA6 matrix still caused a reduction in the material fracture resistance, w_e. In particular, partitioning of w_e in the two components, w_{ey} and

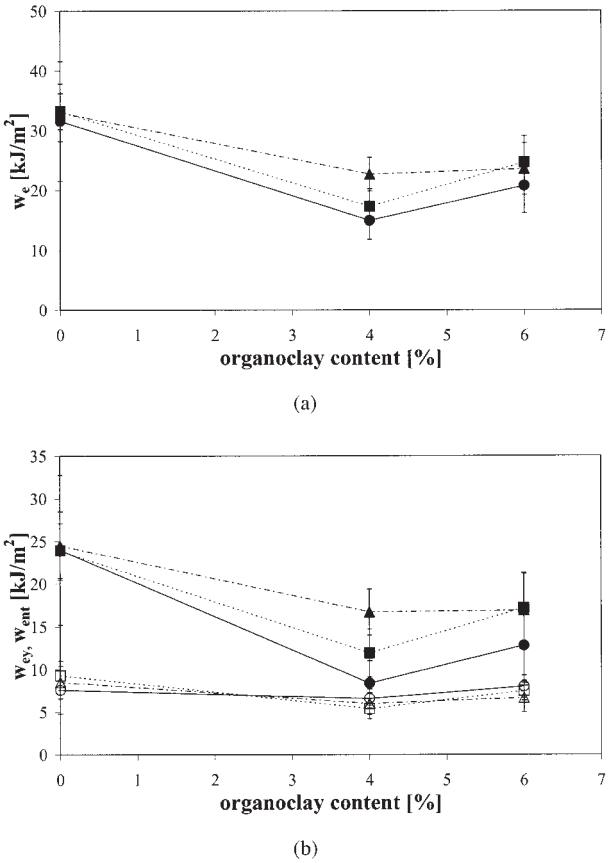

Figure 9 (a) Specific essential work of fracture, w_e (in slightly wet conditions), as a function of organoclay content; (b) yielding component, w_{ey} (open symbols), and necking/tearing component, w_{ent} (solid symbols), of the specific essential work of fracture (in slightly wet conditions) as a function of organoclay content (symbols as in Fig. 6).

w_{ent}, highlighted that the presence of the silicate layers had a considerable influence on the necking/tearing component of the specific essential work of fracture. With a 4% MM content, a 65% reduction was observed for w_{ent} compared to that with PA6, whereas there was only a small effect on the yielding component, w_{ey}. However, the fracture resistance of the nanostructured system containing 6% MM was higher than that of the one containing 4% MM. The addition of the nanofiller into the PA6 matrix caused not only a reduction in the specific essential work of fracture, but also a decrease in the βw_p, which is a global plastic energy dissipation parameter associated with deformation processes that occur in the outer plastic zone away from the fracture surface. This reduction (the βw_p fell from 12.7 to 8.3 MJ/m^3 as MM content increased from 0% to 6%) might indicate that homogeneously dispersed silicate layers impose mechanical constraints on the polymeric matrix, thus limiting large-scale deformations away from the fracture surface.

The results of EWF testing showed that in the two rubber-modified PA6 systems with 5% and 10% rubber content, the incorporation of rubber into the PA6 matrix did not influence either the essential work of fracture contribution, w_e, or the plastic item, βw_p. This means that in wet conditions and at the rate and temperature considered in this study, no appreciable toughening effect was induced in PA6 by the rubbery phase. A possible explanation for this result, which was in contrast with that observed in dry conditions, is that the presence of water molecules adsorbed by PA6 (in the PA6 matrix water acts like a plasticizer) had such a noticeable toughening effect on the polymer matrix that the benefits derived from the addition of a small quantity of rubber (5% and 10%) were substantially overshadowed. The competition between the plastic zone shape factor (β) and the specific nonessential work of fracture (w_p) is the key to understanding the independence of the plastic term, βw_p, from the composition of the rubber-modified systems. The addition of the rubbery phase to PA6 markedly increased the value of the shape factor: the addition of 10% rubber resulted in β increasing by 57%. This means that the incorporation of rubber particles into

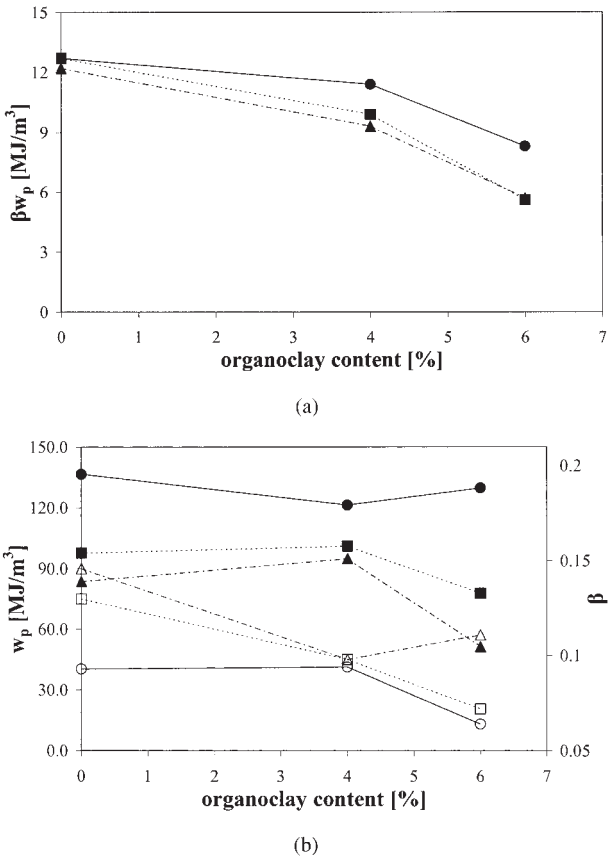

Figure 10 (a) Global plastic energy dissipation parameter, βw_p (in slightly wet conditions), as a function of organoclay content; (b) specific nonessential work of fracture, w_p (solid symbols) and plastic zone shape factor, β (open symbols), in slightly wet conditions, as a function of organoclay content (symbols as in Fig. 6).

TABLE III
Work of Fracture Parameters of the Various Materials in Slightly Wet Conditions

PA6/MM/R[a]							
% MM	% R	w_e (kJ/m^2)	w_{ey} (kJ/m^2)	w_{ent} (kJ/m^2)	βw_p (MJ/m^3)	β (−)	w_p (MJ/m^3)
0	0	31.6 ± 10.0	7.6 ± 2.8	24 ± 8.8	12.7	0.093	136.6
0	5	33.2 ± 3.0	9.3 ± 1.7	23.9 ± 3.2	12.7	0.13	97.7
0	10	33 ± 4.8	8.5 ± 1.9	24.5 ± 4	12.2	0.146	83.6
4	0	15 ± 3.2	6.6 ± 1.1	8.4 ± 2.6	11.4	0.094	121.3
4	5	17.3 ± 3.0	5.4 ± 1.2	11.9 ± 2.8	9.9	0.098	101.0
4	10	22.7 ± 2.8	6 ± 1.3	16.7 ± 2.7	9.3	0.098	94.9
6	0	20.8 ± 4.6	8 ± 1.3	12.8 ± 4.1	8.3	0.064	129.7
6	5	24.7 ± 4.4	7.5 ± 1.1	17.2 ± 4.1	5.6	0.072	77.8
6	10	23.6 ± 4.3	6.7 ± 1.7	16.9 ± 4.3	5.7	0.111	51.4

[a] R, rubber.

the PA6 matrix extended the region involved in plastic deformation during fracture. The increase in β was balanced by the decrease in the specific energy dissipated in the plastic zone outside the fracture process zone (nonessential term, w_p). The addition of 10% rubber to PA6 reduced the value of the plastic energy absorbed per unit volume of the material from 136.6 to 83.6 MJ/m^3. This decrease in the w_p could be justified considering that the plastic behavior of rubber-modified PA6 systems (at 5% and 10% rubber content) seemed to be governed by deformation mechanisms substantially different from those forming the basis of the plastic behavior of neat PA6. This was confirmed by visual analysis of the plastic region generated during the fracture of the DENT specimens, which suggests that in the rubber-modified system with a 10% rubber content, microvoiding occurred, whereas no microvoiding was observed in the neat PA6 except for a very small region at the tip of the notches.

If no significant toughening effect was induced by rubber particles in rubber modified PA6 (in wet conditions), the addition of the rubbery phase to the nanostructured systems increased the fracture resistance, w_e. For the nanostructured system containing 4% MM, the addition of 10% rubber produced a remarkable increase in w_e (51%), whereas for the system containing 6% MM, a a much smaller increase (13%) was observed. The partitioning of w_e into w_{ey} and w_{ent} highlights that the incorporation of rubber into the nanocomposites slightly decreased the yielding component of the specific essential work of fracture, whereas it considerably increased the necking and tearing contribution. For the nanocomposite containing 4% MM, the addition of 10% rubber doubled the w_{ent}, whereas for the system containing 6% MM, a w_{ent} increase of 32% was observed. In contrast with the behavior of rubber-modified PA6, the addition of the rubbery phase to the nanostructured system produced a decrease in the global plastic energy dissipation, βw_p. With an MM content of 6%, the addition of rubber particles induced a remarkable increase in the value of the shape factor: the addition of 10% rubber produced a 73% increase in β. The reduction of the plastic term, βw_p, is therefore a consequence of a large decrease in the specific nonessential work of fracture not counterbalanced by an increase in β (w_p fell from 129.7 to 51.4 MJ/m^3 as rubber content increased from 0% to 10%). A similar behavior also was observed for the nanocomposites containing 4% MM, though no significant change in β was detected. Thus, the reduction of βw_p, with respect to neat PA6, induced by the presence of nanofiller, was made more marked by the incorporation of rubber particles into the system. This effect might be explained by assuming a combined action of rubber particles and silicate layers.

Understanding the deformation mechanisms involved in the rubber-toughening effects observed in the systems investigated requires an extensive and systematic investigation of material phase morphology. This work is in progress.

CONCLUSIONS

PA6-based nanocomposites with a high level of exfoliation were prepared via melt blending. The presence of silicate layers in the PA6 matrix strongly influenced the yield and fracture behavior of the material, increasing the yield stress but reducing the fracture resistance, depending on the humidity content. The addition of a rubbery phase increased the fracture resistance of the nanocomposites in slightly wet conditions, providing evidence of a toughening effect, whereas no significant increase in fracture toughness was observed in the materials in dry conditions. In addition, the results show that, for given humidity conditions, a good balance between stiffness and toughness is obtainable by employing a suitable ratio of rubber–to–silicate layers content.

The authors are grateful to Dr. A. Filippi and Ing. S. Gatti of Radici Novacips SpA (Villa d'Ogna, Bergamo, Italy) for the materials kindly supplied and to Dr. M. Ferroni of Dipartimento di Chimica e Fisica per l'Ingegneria e per i Materiali of Università di Brescia (Italy) for the SEM analyses.

References

1. Usuki, A.; Kojima, Y.; Kawasumi, M.; Okada, A.; Fukushima, Y.; Kurauch, T.; Kamigaito, O. J Mater Res 1993, 8, 1179.
2. Alexandre, M.; Dubois, P. Mater Sci Eng R-Rep 2000, 28, 1.
3. Lincoln, D. M.; Vaia, R. A.; Wang, Z.-G.; Hsiao, B. S.; Krishnamoorti, R. Polymer 2001, 42, 9975.
4. Varlot, K.; Reynaud, E.; Kloppfer, M. H.; Vigier, G.; Varlet, J. J Polym Sci, Part B: Polym Phys 2001, 39, 1360.
5. Masanelli-Varlot, K.; Reynaud, E.; Vigier, G.; Varlet, J. J Polym Sci, Part B: Polym Phys 2002, 40, 272.
6. Liu, T. X.; Liu, Z. H.; Ma, K. X.; Shen, L.; Zeng, K. Y.; He, C. B. Compos Sci Technol 2003, 63, 331.
7. Liu, L.; Qi, Z.; Zhu, X. J Appl Polym Sci 1999, 71, 1133.
8. Cho, J. W.; Paul, D. R. Polymer 2001, 42, 1083.
9. Dennis, H. R.; Hunter, D. L.; Chang, D.; Kim, S.; White, J. L.; Cho, J. W.; Paul D. R. Polymer 2001, 42, 9513.
10. Usuki, A.; Koiwai, A.; Kojima, Y.; Kawasumi, M.; Okada, A.; Kurauch, T.; Kamigaito, O. J Appl Polym Sci 1995, 55, 119.
11. Nair, S. V.; Goettler, L. A.; Lysek, B. A. Polym Eng Sci 2002, 42, 1872.
12. Yu, Z. Z.; Yan, C.; Yang, M.; Mai, Y.-W. Polym Int 2004, 53, 1093.
13. ISO 13586. Plastics—Determination of Fracture Toughness (G_{Ic} and K_{Ic})—Linear Elastic Fracture Mechanics (LEFM) Approach; 2000.
14. Clutton, E.; Moore, R. Essential Work of Fracture and Cohesive Zone Fracture Toughness, ESIS-TC4 Test Protocol, 2002.
15. Broberg, K. B. Int J Fract 1968, 1, 19.
16. Mai, Y.-W.; Cotterell, B. Int J Fract 1986, 32, 105.
17. Arkhireyeva, A.; Hashemi, S.; O'Brien, M. J Mater Sci 1999, 34, 5961.
18. Hashemi, S.; Williams, J. G. Plast Rubber Compos 2000, 29, 294.
19. Arkhireyeva, A.; Hashemi, S. Eng Fract Mech 2004, 71, 789.
20. Kohan, M. I. Nylon Plastics Handbook; Hanser Verlag: Munich, Vienna, New York, 1995.
21. Baldi, F.; Bignotti, F.; Tieghi, G.; Riccò, T. In preparation.
22. Khatua, B. B.; Lee, D. J.; Kim, H. Y.; Kim, J. K. Macromolecules 2004, 37, 2454.
23. Gray, A. Testing Protocol for Essential Work of Fracture, ESIS-TC4 Test Protocol, 1993.
24. Heino, M.; Hietaoja, P.; Seppälä, J.; Harmia, T.; Friedrich, K. J Appl Polym Sci 1997, 66, 2209.
25. Karger-Kocsis, J.; Czigány, T.; Moskala, E. J. Polymer 1998, 39, 3939.
26. Ferrer-Balas, D.; Maspoch, M. L.; Martinez, A. B.; Santana, O. O. Polym Bull 1999, 42, 101.
27. Ferrer-Balas, D.; Maspoch, M. L.; Martinez, A. B.; Santana, O. O. Polymer 2001, 42, 1697.
28. Ferrer-Balas, D.; Maspoch, M. L.; Martinez, A. B.; Ching, E.; Li, R. K. Y.; Mai, Y.-W. Polymer 2001, 42, 2665.